COMMUNICATION

Check for updates

Realizing fast Li-ion conduction of Li_3PO_4 solid electrolyte at low temperature by mechanochemical formation of lithium-containing dual-shells†

Shunqin Zeng,[ab] Xiaoli Ding, [ORCID] *[a] Liqing He,[c] Hai-Wen Li, [ORCID] *[c] Qingan Zhang[a] and Yongtao Li[ad]

Dual lithium-containing hydride/oxide shells are constructed by *in situ* mechano-induced assembly of Li_3PO_4 reacting with $LiBH_4$. The ionic conductivity of the Li_3PO_4-based composite is promoted nearly 4 orders of magnitude, up to 0.04 mS cm^{-2} at 75 °C as compared to the pure one, possessing an electrochemical window of -0.2–5 V (*vs.* Li/Li$^+$).

As an efficient energy storage device, rechargeable lithium-ion batteries (LIBs) play an important role in replacing fossil fuels that cause environmental pollution.[1] Commercial liquid lithium-ion batteries are widely used in micro-electronic products, hybrid electric vehicles, grid energy conversion storage systems and other energy storage fields.[2–4] However, they can lead to safety issues as they use volatile liquid electrolytes, which are flammable and explosive.[5,6] At present, it is urgent to develop safe and reliable batteries with high storage energy density, long cycle life and low price. To solve the above-mentioned problem, all-solid-state batteries have been designed where high-capacity lithium metal acts as the anode and the organic liquid electrolytes are replaced by safe and stable solid electrolytes (SSEs).[7,8] The key issues of the electrolyte of all-solid-state batteries depend on the employment of new electrolyte materials, possessing high ion conductivity, and good electrochemical and mechanical stability at room temperature.[9,10]

a School of Materials Science and Engineering & Low-Carbon New Materials Research Center, Anhui University of Technology, Maanshan 243002, China. E-mail: dingxiaoli@ahut.edu.cn
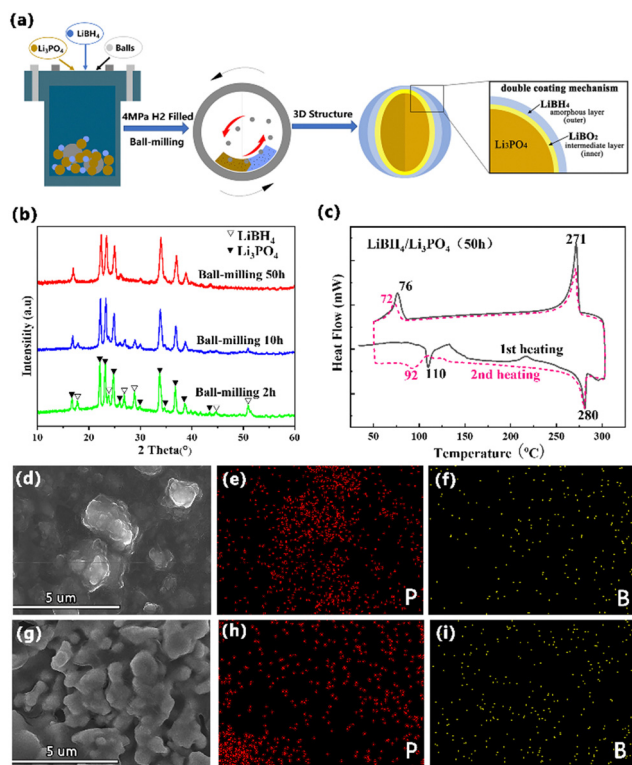
b Hunan Engineering Laboratory for Preparation Technology of Polyvinyl Alcohol Fiber (PVA) Material, Huaihua University, Huaihua, 418000, China

c Hefei General Machinery Research Institute, Hefei, Anhui 230031, P. R. China. E-mail: lihaiwen66@hotmail.com

d Key Laboratory of Green Fabrication and Surface Technology of Advanced Metal Materials of Ministry of Education, Anhui University of Technology, Maanshan 243002, China

† Electronic supplementary information (ESI) available: Experimental details, DSC curves, EIS, Arrhenius diagram and specific surface area for the $LiBH_4$/Li_3PO_4 composite. See DOI: https://doi.org/10.1039/d3ma00125c

So far, extensive research has been conducted on SSEs covering polymer materials and inorganic materials.[11,12] Among them, the typical conductive polymers are polyoxyethylene (PEO),[13] polyacrylonitrile (PAN),[14] polymethyl methacrylate (PMMA)[15] and polyvinylidene difluoroethylene (PVDF),[16] and the typical inorganic conductive materials include glass/ceramic,[17] garnets,[18] sulfides,[19] perovskites[20] and hydrides.[21] Despite extensive research and significant progress in solid electrolytes over the past few decades, there are currently no commercially available battery solutions to meet the requirements of production and daily life.[22,23] The main challenge at present is to develop new solid electrolytes with facile preparation processes and excellent electrochemical performance, possessing high lithium ion conductivity.[24]

As a typical glassy material, Li_3PO_4 takes advantages of low cost, easy preparation, environmental inertness, and negligible electron conductivity.[25–27] Therefore, it has been widely applied in improving the electro-chemical properties of lithium-rich electrode materials[28] and inhibiting the growth of lithium dendrites in lithium metal batteries.[29] However, the application of Li_3PO_4 in solid electrolytes is barely reported because of its much lower conductivity of 10^{-10} S cm^{-1} at room temperature (RT).[25]

Herein, we propose the technique of surficial modification of Li_3PO_4 particles by introducing lithium borohydride ($LiBH_4$) to achieve high ionic conductivity and good electro-chemical properties. The $LiBH_4$ as a fast-ion conductive solid electrolyte was first reported by Matsuo *et al.*, which shows good electrochemical stability and good interface compatibility with electrode materials.[30,31] It was found that the prepared $LiBH_4$/Li_3PO_4 composite had a double-coated structure, namely, $LiBO_2$ as the intermediate layer to prevent further reaction between $LiBH_4$ and Li_3PO_4, and the amorphous $LiBH_4$ as an outer layer to provide a continuous ionic conductivity network among Li_3PO_4 particles to synergistically improve their ionic conductivity. The composites presented an ionic conductivity up to 0.04 mS cm^{-2} at 75 °C, which is nearly 4 orders of magnitude higher than that of pure Li_3PO_4. Moreover, the solid electrolyte of $LiBH_4$/Li_3PO_4 composites

Fig. 1 (a) The preparation schematic diagram of LiBH$_4$/Li$_3$PO$_4$ composites with a dual-layer structure; (b) X-ray diffraction patterns of the 50 wt% LiBH$_4$/Li$_3$PO$_4$ composite with different milling times; (c) *in situ* DSC curves of the 50 wt% LiBH$_4$/Li$_3$PO$_4$ composite by heating/cooling; SEM image and EDS mapping of 50 wt% LiBH$_4$/Li$_3$PO$_4$ milled for 2 h (d)−(f) and 50 h (g)−(i), respectively.

exhibited excellent electro-chemical properties, such as a wide electro-chemical window (5 V *vs.* Li/Li$^+$) and negligible number of electron migrations. These results provide new possibilities for developing suitable SSEs with excellent ionic conductivity.

The lithium-contained dual shells of Li$_3$PO$_4$ electrolyte were assembled by one-step ball milling (Fig. 1a). According to the X-ray diffraction (XRD) patterns in Fig. 1b, the diffraction peaks of Li$_3$PO$_4$ keep stable while the peak strength of LiBH$_4$ gradually weakens with the increase of the milling time from 2 h to 50 h, indicating that the grain size becomes refined. The thermal stability of the 50 wt% LiBH$_4$/Li$_3$PO$_4$ composite as a model was further studied by *in situ* differential calorimetry. From (Fig. 1c and Fig. S1a, ESI†), it can be seen that endothermic and exothermic peaks are observed on each differential scanning calorimeter (DSC). The endothermic peak at about 110 °C and the exothermic peak at ∼76 °C correspond to the phase transition temperature of LiBH$_4$ from *Pnma* to *P6$_3$mc*,[30] while the exothermic peak observed at ∼280 °C and the endothermic peak observed at ∼270 °C represent its melting and re-crystallization process. The second cycle of differential scanning calorimeter exhibits a similar tendency though a slight shift in temperature curve. These results confirm that the LiBH$_4$/Li$_3$PO$_4$ composites are thermally stable at a temperature range of 308–573 K, which would help the all-solid-state battery maintain stability in a high-temperature environment.

Fig. 1(d–i) shows the scanning electron microscope (SEM) images and Energy Dispersive Spectrometer (EDS) mapping of the 50 wt% LiBH$_4$/Li$_3$PO$_4$ composites with the milling time of 2 h and 50 h, respectively. It can be seen that the introduction of LiBH$_4$ caused obvious agglomeration and adhesion of the particles. On magnified observation, we found that some of the sample particles exhibited an encapsulated morphology, which may be due to the formation of a low Young's modulus LiBH$_4$ covering layer around high Young's modulus Li$_3$PO$_4$ particles.[32,33] This is further confirmed by the EDS mappings of highly dispersed B and P elements.

To gain a deeper understanding of the sample micro-structure, transmission electron microscope (TEM) and X-ray photoelectron spectroscopy (XPS) surface sputtering techniques were conducted. From the TEM image and the corresponding selected electron diffraction pattern (Fig. 2a–d), it can be seen that the sample has a dual-layer structure, where the amorphous coating corresponds to LiBH$_4$, the lattice fringes correspond to the (010) intermediate layer LiBO$_2$ and the interplanar spacing of 0.3078 nm belongs to the (111) crystal plane of the Li$_3$PO$_4$ core, respectively (Fig. 2d and e). Fig. 2(g and h) show the XPS depth profiling plots of elements B and Li in the samples before and after sputtering, respectively. The peaks located at 187.8 eV and 191.7 eV in the high-resolution B 1s XPS spectrum before sputtering correspond to the B–H bonds[34] in LiBH$_4$ and the B–O bonds in LiBO$_2$,[35] respectively, and the relative intensity of the characteristic peaks of LiBO$_2$ in the B^{1s} spectrum is further enhanced after 15 s sputtering. The high-
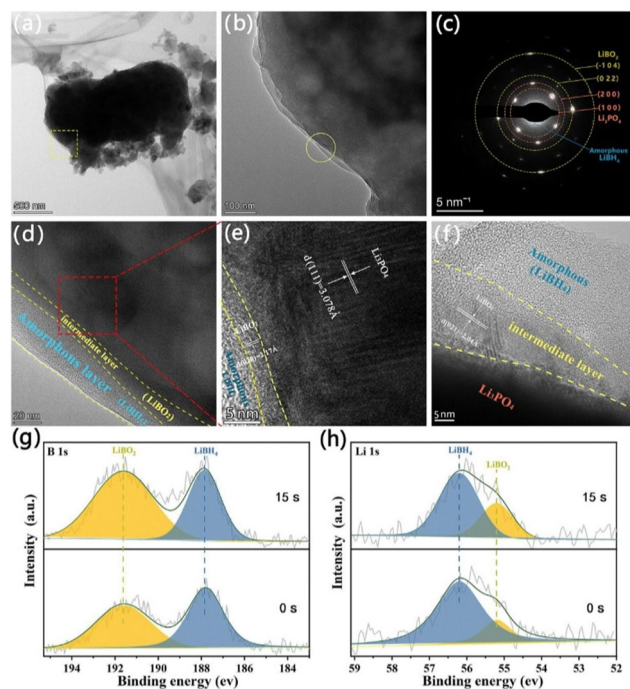
Fig. 2 (a) and (b) TEM images and (c) its SAED pattern b, as well as (d)−(f) HRTEM images of 50 wt% LiBH$_4$/Li$_3$PO$_4$ composites; and high resolution XPS spectra of (g) B^{1s} and (h) Li^{1s} before and after etching for different times.

resolution Li 1s characteristic peaks corresponding to $LiBH_4$ (~ 56.2 eV) and $LiBO_2$ (~ 55.2 eV) also appear in the XPS spectrum,[33] and the relative content of $LiBO_2$ and the relative content of $LiBH_4$ gradually decrease after sputtering for 15 s. Combining the TEM and XPS results, we found that the cladding layer formed around the Li_3PO_4 particles is a bilayer structure composed of $LiBH_4$ as the outer layer and $LiBO_2$ as the intermediate layer. $LiBH_4$ as an amorphous provides more lithium-ion transmission channels and continuous ion-guided circuits for the Li_3PO_4, while $LiBO_2$ as the intermediate layer plays a role in preventing $LiBH_4$ and Li_3PO_4 from continuous reaction in the ball-milling process. Therefore, the formation of the cladding layer not only improves the ionic conductivity of Li_3PO_4 but also enhance their cold-working formability.

In order to determine the Li^+ ion conductivity, the as-milled $LiBH_4/Li_3PO_4$ composite was cold pressed into pellets at room temperature and then held for 8 h subjected to electrochemical impedance spectra (EIS) examination. It could be found that the longer the ball grinding time, the smaller the impedance of the sample at room temperature (Fig. 3a). The ion conductivity curves of the sample with different milling times are shown in Fig. 3b. Compared with the 50 wt% $LiBH_4/Li_3PO_4$ composite material ground for 2 h at room temperature, the ion conductivity of the 50 wt% $LiBH_4/Li_3PO_4$ composite material ground for 50 h increased by nearly an order of magnitude. In addition, the activation energy (E_a) of lithium-ion mobility can be quantitatively analyzed by linear fitting of the data in Fig. 3b by using Arrhenius eqn (1):[31]

$$\ln \sigma T = -\frac{E_a}{K_B T} + C \qquad (1)$$

where K_B stands for Boltzmann's constant and C stands for the constant. The Arrhenius calculation results are shown in Fig. 3c. As the milling time prolongs, the activation energy of the sample gradually decreases, which is due to the finer grain size leading to a lower activation energy interface that can provide for lithium-ion conduction. This is also confirmed by the Brunauer–Emmett–Teller

(BET) method testing of three sets of samples with different lengths of ball-milling time (Fig. S4, ESI†). As shown in Fig. 3d, the activation energy gradually decreases with extending the milling time, which is an effective way to improve the ion conductivity.

The direct current polarization curve of SUS|50 wt% $LiBH_4/Li_3PO_4$|SUS symmetrical batteries was measured at 105 °C. As shown in Fig. 4a, the discharge current drops sharply after applying a 10 mV step voltage and then tends to stabilize. The electron conductivity (σ_e) of the sample is calculated using eqn (2):[31]

$$\sigma_e = \frac{I_0 d}{U_0 S} \qquad (2)$$

where I_0 is the steady-state current, d is the electrolyte sheet thickness, U_0 is the applied voltage, and S is the surface area of the electrolyte sheet. The electron conductivity of the sample was calculated to be about 1.176×10^{-7} S cm^{-1}, which was about 2 orders of magnitude lower than the conductivity of lithium-ions at the same temperature, and the lithium-ion mobility was determined to be greater than 0.99. This strongly indicates that the 50 wt% $LiBH_4/Li_3PO_4$ composite solid electrolyte is a typical single-ion conductor and the electron conduction is negligible, which would help to improve the cycling performance of the solid electrolyte and the inhibition of lithium dendrites. Fig. 4b shows that the Li|50 wt% $LiBH_4/Li_3PO_4$ |SUS battery is swept from the starting voltage -0.2 V to the termination voltage 5 V, with corresponding cyclic voltammetry (CV) curves at 105 °C at a sweep rate of 5 mV s^{-1} (a total of 5 turns). From the CV curve it can be seen that no other significant red-dotted peaks were observed in
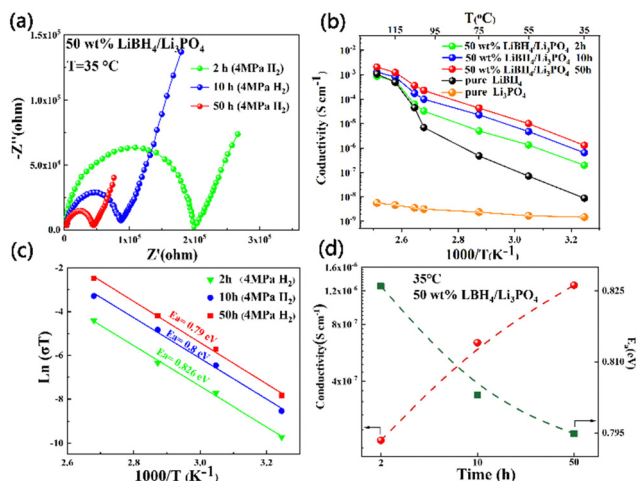

Fig. 3 (a)–(c) Ion transport characteristics of the 50 wt% $LiBH_4/Li_3PO_4$ composite under different ball milling times; and (d) the relationship between ionic conductivity and milling time.
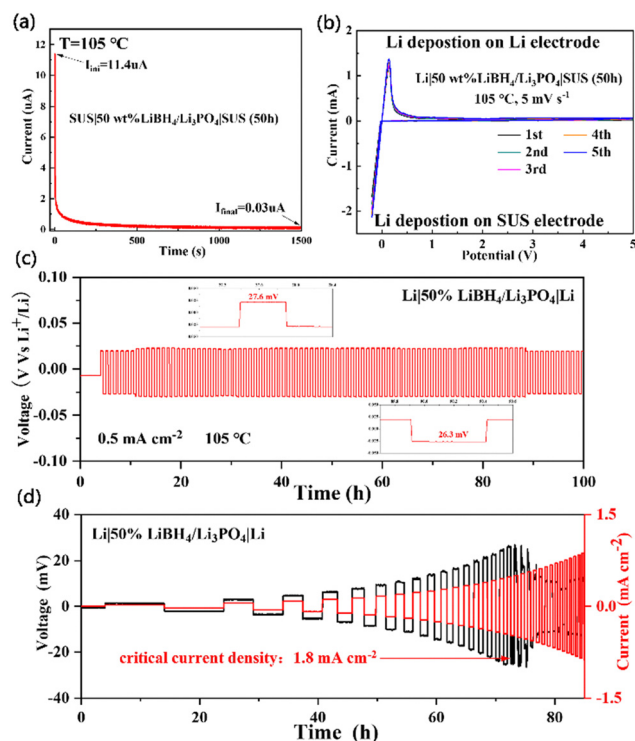

Fig. 4 (a) DC polarization curve, (b) cyclic voltammetry curve, (c) constant current cycle curve and (d) stepped current density galvanostatic cycle of the 50 wt% $LiBH_4/Li_3PO_4$ composite.

the de-embedding lithium current peaks (observed near 0 V in the wide voltage window of -0.5–5 V), which indicates that the 50 wt% $LiBH_4/Li_3PO_4$ composite solid electrolyte has a wide electrochemical window.

The cycling performance of the 50 wt% $LiBH_4/Li_3PO_4$ composite solid electrolytes and the inhibition ability of lithium dendrites were further evaluated. At 105 °C, we applied to the Li|50wt% $LiBH_4/Li_3PO_4$|Li symmetrical battery a constant current of 0.5 mA/cm^{-2} and a step current density of 0.1 mA cm^{-2} as the starting current and 0.1 mA cm^{-2} as the step length. As is shown in Fig. 4c, the battery has no significant voltage fluctuations within 100 cycles, which proves that the 50 wt% $LiBH_4/Li_3PO_4$ composite solid electrolyte has good electro-chemical cycling stability after ball-milling for 50 h. In addition, the limited current density of the Li|50wt% $LiBH_4/Li_3PO_4$|Li battery is determined to be 1.8 mA cm^{-2} (Fig. 4d), which corresponds to the critical current density for lithium dendrite formation and the above results indicate that the stable interphase between Li and $LiBH_4/Li_3PO_4$ can effectively suppress the growth of Li dendrites. This remarkable cycling performance can be attributed to two factors including the stable surface contact among particles due to the filling of the amorphous outer layer of $LiBH_4$ providing a continuous ionic conductive network between Li_3PO_4 particles and the extremely low electronic conductivity that effectively suppresses the growth of Li dendrites.[36]

In summary, we developed an effective strategy to improve the lithium-ion conductivity of the Li_3PO_4-based solid-state electrolyte, namely, the $LiBH_4/Li_3PO_4$ solid-state electrolyte constructed by in-situ mechano-chemical reaction, which exhibits a bilayer structure: (i) the formed $LiBO_2$ as an intermediate layer will prevent further reactions between $LiBH_4$ and Li_3PO_4, (ii) the amorphous outer layer of $LiBH_4$ can provide a continuous ionic conductive network between Li_3PO_4 particles. The $LiBH_4/Li_3PO_4$ (50 wt%) composite exhibits an excellent ion conductivity of 0.04 m S cm^{-2} at 75 °C. This is mainly due to the amorphous $LiBH_4$ outer layer providing more lithium ion transfer channels and fine particles resulting in lower energy interfaces for lithium ion conduction. In addition, the $LiBH_4/Li_3PO_4$ electrolyte also exhibits a wide electro-chemical stability window, excellent cycling stability and strong lithium dendrite inhibition. These findings can provide an alternative route to improve the ion conductivity of solid electrolytes in all-solid-state batteries.

Conflicts of interest

There are no conflicts to declare.

Notes and references

1 S. Chu and A. Majumdar, *Nature*, 2012, **488**, 294–303; M. Armand and J. M. Tarascon, *Nature*, 2008, **451**, 652–657.

2 Y. Kato, S. Hori, T. Saito, K. Suzuki, M. Hirayama, A. Mitsui, M. Yonemura, H. Iba and R. Kanno, *Nat. Energy*, 2016, **1**, 16030; J. W. Choi and D. Aurbach, *Nat. Rev. Mater.*, 2016, **1**, 16013.

3 N. Kamaya, K. Homma, Y. Yamakawa, M. Hirayama, R. Kanno, M. Yonemura, T. Kamiyama, Y. Kato, S. Hama, K. Kawamoto and A. Mitsui, *Nat. Mater.*, 2011, **10**, 682–686.

4 Z. Yang, J. Zhang, M. C. W. Kintner-meyer, X. Lu, D. Choi, J. P. Lemmon and J. Liu, *Chem. Rev.*, 2011, **111**, 3577–3613.

5 Q. Wang, L. Jiang, Y. Yu and J. Sun, *Nano Energy*, 2019, **55**, 93–114; Y. Zhao, K. Zheng and X. Sun, *Joule*, 2018, **2**, 2583–2604.

6 S. Mao, Q. Wu, F. Ma, T. Wu and Y. Lu, *Chem. Commun.*, 2021, **57**, 840–857.

7 Z. Piao, P. Xiao, R. Luo, J. Ma, R. Gao, C. Li, J. Tan, K. Yu, G. Zhou and H. Cheng, *Adv. Mater.*, 2022, **34**, 2108400.

8 Q. Zhao, S. Stalin, C. Z. Zhao and L. A. Archer, *Nat. Rev. Mater.*, 2020, **5**, 229–252.

9 Y. Xiao, Y. Wang, S.-H. Bo, J. Kim, L. J. Miara and G. Ceder, *Nat. Rev. Mater.*, 2020, **5**, 105–126.

10 X. Chen, C. Zhao, Y. Yao, H. Liu and Q. Zhang, *Chemistry*, 2019, **5**, 74–96.

11 X. Liu, X. Li, H. Li and H. Wu, *Chem. – Eur. J.*, 2018, **24**, 18293–18306.

12 T. Zhang, W. He, W. Zhang, T. Wang and P. Li, *Chem. Sci.*, 2020, **11**, 8686–8707.

13 Q. Zhou, J. Ma, S. Dong, X. Li and G. Cui, *Adv. Mater.*, 2019, **31**, 1902029.

14 Y. Shuai, Z. Zhang, K. Chen, J. Lou and Y. Wang, *Chem. Commun.*, 2019, **55**, 2376–2379.

15 S. Venkatesan, I. P. Liu, J. Lin, M. Tsai, H. Teng and Y. Lee, *J. Mater. Chem. A*, 2018, **6**, 100856.

16 Y. Shan, L. Li, X. Chen, S. Fan, H. Yang and Y. Jiang, *ACS Energy Lett.*, 2022, **7**, 2289–2296.

17 X. Chi, Y. Zhang, F. Hao, S. Kmiec, H. Dong, R. Xu, K. Zhao, Q. Ai, T. Terlier, L. Wang, L. Zhao, L. Guo, J. Lou, H. Xin, S. W. Martin and Y. Yao, *Nat. Commun.*, 2022, **13**, 2854.

18 R. Murugan, V. Thangadurai and W. Weppner, *Angew. Chem., Int. Ed.*, 2007, **46**, 7778–7781; J. Zhang, C. Wang, M. Zheng, M. Ye, H. Zhai, J. Li, G. Tan, X. Tang and X. Sun, *Nano Energy*, 2022, **102**, 107672.

19 Y. Lee, J. Jeong, H. Lee, M. Kim, D. Han, H. Kim, J. Yuk, K. Nam, K. Chung, H. Jung and S. Yu, *ACS Energy Lett.*, 2022, **7**, 171–179; J. Xu, Y. Li, P. Lu, W. Yan, M. Yang, H. Li, L. Chen and F. Wu, *Adv. Mater.*, 2021, **13**, 2102348; P. Lu, L. Li, S. Wang, J. Xu, J. Peng, W. Yan, Q. Wang, H. Li, L. Chen and F. Wu, *Adv. Mater.*, 2021, **33**, 210096.

20 Q. Zhang, N. Schmidt, J. Lan, W. Kim and G. Cao, *Chem. Commun.*, 2014, **50**, 5593–5596.

21 H. Liu, Z. Ren, X. Zhang, J. Hu, M. Gao, H. Pan and Y. Liu, *Chem. Mater.*, 2019, **32**, 671–678.

22 J. Zhang, X. Zang, H. Wen, T. Dong, J. Chai, Y. Li, B. Chen, J. Zhao, S. Dong, J. Ma, L. Yue, Z. Liu, X. Guo, G. Cui and L. Chen, *J. Mater. Chem. A*, 2017, **5**, 4940–4948.

23 R. Chen, Q. Li, X. Yu, L. Chen and H. Li, *Chem. Rev.*, 2020, **120**, 6820–6877.

24 E. Quartarone and P. Mustarelli, *Chem. Soc. Rev.*, 2011, **40**, 2525–2540.

25 F. Lu, Y. Pang, M. Zhu, F. Han, J. Yang, F. Fang, D. Sun, S. Zheng and C. Wang, *Adv. Funct. Mater.*, 2019, **29**, 1809219.

26 E. Kartini, M. Nakamura, M. Arai, Y. Inamura, K. Nakajima, T. Maksum, W. Honggowiranto and T. Y. S. P. Putra, *Solid State Ion*, 2014, **262**, 833–836.

27 L. D. Prayogi, M. Faisal, E. Kartini, W. Honggowiranto and C. Supardi, *AIP Conf. Proc.*, 2016, **1710**, 030047; M. B. Bechir and A. B. Rhaiem, *Phys. E*, 2021, **130**, 114686.

28 B. Xu, W. Li, H. Duan, H. Wang, Y. Guo, H. Li and H. Liu, *J. Power Sources*, 2017, **354**, 68–73.

29 N. D. Lepley, N. A. W. Holzwarth and Y. A. Du, *Phys. Rev. B: Condens. Matter Mater. Phys.*, 2013, **88**, 104103.

30 H. Maekawa, M. Matsuo, H. Takamura, M. Ando, Y. Noda, T. Karahashi and S. Orimo, *J. Am. Chem. Soc.*, 2009, **131**(3), 894–895.

31 Z. Wu, K. Wang, W. Sun, Z. Li, Z. Ma, Y. Zhu, Y. Zou and Y. Zhang, *Adv. Funct. Mater.*, 2022, 2205677.

32 N. Li, Y. Yin, C. Yang and Y. Guo, *Adv. Mater.*, 2016, **28**(9), 1853–1858.

33 Y. Gao, S. Sun, X. Zhang, Y. Liu, J. Hu, Z. Huang and M. Gao, *Adv. Funct. Mater.*, 2021, **31**(15), 2009692.

34 E. Deprez, M. A. Muñoz-Márquez, M. C. Jimenez de Haro, F. J. Palomares, F. Soria, M. Dornheim, R. Bormann and A. Fernández, *J. Appl. Phys.*, 2011, **109**(1), 014913.

35 D. A. Hensley and S. H. Garofalini, *Appl. Surf. Sci.*, 1994, **81**(3), 331–339.

36 C. Tsai, V. Roddatis, C. V. Chandran, Q. Ma, S. Uhlenbruck, M. Bram, P. Heitjans and O. Guillon, *ACS Appl. Mater. Interfaces*, 2016, **8**(16), 10617.